Behavioral/Systems/Cognitive

Polarization-Sensitive Descending Neurons in the Locust: Connecting the Brain to Thoracic Ganglia

Ulrike Träger and Uwe Homberg
Fachbereich Biologie, Tierphysiologie, Philipps-Universität Marburg, D-35032 Marburg, Germany

Many animal species, in particular insects, exploit the *E*-vector pattern of the blue sky for sun compass navigation. Like other insects, locusts detect dorsal polarized light via photoreceptors in a specialized dorsal rim area of the compound eye. Polarized light information is transmitted through several processing stages to the central complex, a brain area involved in the control of goal-directed orientation behavior. To investigate how polarized light information is transmitted to thoracic motor circuits, we studied the responses of locust descending neurons to polarized light. Three sets of polarization-sensitive descending neurons were characterized through intracellular recordings from axonal fibers in the neck connectives combined with single-cell dye injections. Two descending neurons from the brain, one with ipsilaterally and the second with contralaterally descending axon, are likely to bridge the gap between polarization-sensitive neurons in the brain and thoracic motor centers. In both neurons, *E*-vector tuning changed linearly with daytime, suggesting that they signal time-compensated spatial directions, an important prerequisite for navigation using celestial signals. The third type connects the suboesophageal ganglion with the prothoracic ganglion. It showed no evidence for time compensation in *E*-vector tuning and might play a role in flight stabilization and control of head movements.

Introduction

Many insects, crustaceans, arachnids, and representatives of several vertebrate taxa are able to detect the polarization pattern of the blue sky and use it, in addition to direct sunlight, for navigational tasks (Horváth and Varjú, 2004; Wehner and Labhart, 2006). At the neuronal level, polarization vision pathways in the brain have been studied most extensively in locusts and crickets (Labhart and Meyer, 2002; Homberg, 2004). In these insects, the central complex is a major processing stage for polarized light (Vitzthum et al., 2002; Heinze and Homberg, 2007, 2009; Sakura et al., 2008; Heinze et al., 2009). Heinze and Homberg (2009) showed that polarization-sensitive (POL-) neurons connect the central complex to the lateral accessory lobes and the posterior protocerebrum, brain areas that are innervated by intersegmental neurons (Williams, 1975; Strausfeld and Seyan, 1985; Okada et al., 2003). Although polarization-mediated behavior in insects has been studied extensively (bees and ants: Wehner and Rossel, 1985; Wehner, 2003; crickets: Brunner and Labhart, 1987; Henze and Labhart, 2007; flies: von Philipsborn and Labhart, 1990; beetles: Dacke et al., 2003; locusts: Mappes and Homberg, 2004; butterflies: Reppert et al., 2004), the anatomical and functional connections from POL-neurons in the brain to thoracic motor centers have not been explored in any species.

Descending neurons mediate behaviorally relevant signals from the brain to motor circuits in the thoracic ganglia. They modify the activity of thoracic networks to adapt specific behaviors depending on current stimulus conditions. Previous studies on descending visual neurons have analyzed looming-sensitive neurons mediating escape (Rind et al., 2008; Fotowat et al., 2009; Yamawaki and Toh, 2009), deviation detector neurons controlling flight balance (Griss and Rowell, 1986; Rowell and Reichert, 1986; Hensler, 1988, 1992; Hensler and Rowell, 1990), neurons coding for self-motion (Wertz et al., 2008, 2009a,b), target-selective neurons mediating prey detection (Olberg, 1986; Frye and Olberg, 1995), and figure-detecting neurons involved in flower recognition (Sprayberry, 2009). Descending neurons mediating sky compass-related polarization information should encode two important factors: the position of the sun and the daytime. The polarization pattern of the blue sky is fixed to the position of the sun and, therefore, changes during the day as the sun moves across the sky. Animals that use the sun or polarization pattern for navigation have to compensate that shift, based on daytime information and knowledge of the local solar ephemeris function. Pfeiffer and Homberg (2007) showed that neurons of the anterior optic tubercle of the locust brain compensate for changes in sky polarization associated with changing solar elevation, but the sites and mechanisms underlying compensation for daytime shifts in solar azimuth are still unclear.

The present study used intracellular recordings to identify and characterize polarization-sensitive descending neurons in the desert locust. Three types of POL-neurons were characterized. Two of these cell types show evidence for time compensation in solar azimuth coding. The data complement our understanding

Received July 12, 2010; revised Nov. 26, 2010; accepted Dec. 2, 2010.

This work was supported by Deutsche Forschungsgemeinschaft Grant HO 950/18-1. We are grateful to Dr. Klaus Hensler for technical advice on neck connective recordings. We thank Dr. Keram Pfeiffer for providing Spike2-scripts for data analysis, Dr. Stanley Heinze and Basil el Jundi for contributing physiological data on four descending neurons, and Drs. Eve Marder, Hans Agricola, and Heinrich Dircksen for the donation of antisera. We are grateful to Sebastian Richter and Manfred Peil for constructing the stimulation devices and control equipment and to Karl Heinz Herklotz and Martina Kern for raising desert locusts.

Correspondence should be addressed to Uwe Homberg, Fachbereich Biologie, Tierphysiologie, Universität Marburg, D-35032 Marburg, Germany. E-mail: homberg@staff.uni-marburg.de.

DOI:10.1523/JNEUROSCI.3624-10.2011

Copyright © 2011 the authors 0270-6474/11/312238-10$15.00/0

of the polarization vision system in the locust and open the door to future analysis of polarized-light-dependent thoracic motor circuits.

Materials and Methods

Preparation of animals. Locusts (*Schistocerca gregaria*) raised under 12 h light/dark photoperiod, 50% relative humidity, and a temperature cycle of 28°C during the night and 35°C during the day were taken from crowded colonies at the University of Marburg. Adult animals of both sexes were used 1–3 weeks after imaginal moult. They were anesthetized by cooling for 15–30 min and waxed onto a metal holder in horizontal position. In some cases, the tibiae of the hindlegs were cut off. A 3 × 5 mm window was cut dorsally into the pronotum. After removal of gut, tracheal air sacs, fat bodies, and the tissue membrane between gut and ventral body cavity, the neck connectives between suboesophageal ganglia (SOG) and prothoracic ganglia (Pro-TG) were exposed. Using a glass hook, the neck connectives were manipulated into two grooves of a rectangular platform (1 × 2 mm) made of platinum. The connectives were submersed in locust saline at all times to prevent desiccation (Clements and May, 1974).

Electrophysiology. For intracellular recordings, microelectrodes (resistance, 10–50 MΩ) were pulled from borosilicate capillaries (0.75 mm inner diameter, 1.5 mm outer diameter; Hilgenberg) using a Flaming/Brown horizontal puller (P-97; Sutter Instruments). Their tips were either filled with a 3% aqueous solution of fluorescent dextran (Alexa Fluor 488 or 647; 10,000 molecular weight, anionic, fixable; Invitrogen) or with 4% Neurobiotin (Vector Laboratories) in 1 M KCl and backed up with 1 M KCl. Intracellular signals were amplified (10×) with a custom-made amplifier and monitored with an audio monitor and a digital oscilloscope (Hameg HM 305; Hameg). After sampling at a rate of 10 kHz with a Digidata 1322A (Molecular Devices), signals were stored on a personal computer using pClamp9 software (Molecular Devices). Some recordings were digitally high-pass filtered to compensate for shifts in baseline. After recording, the tracer was injected iontophoretically into the cell with constant hyperpolarizing current (2–10 nA for 1–36 min, dextran) or constant depolarizing current (2–7 nA for 1–65 min, Neurobiotin). Under stable conditions, recordings lasted for ~20–30 min.

Visual stimulation. For visual stimulation, a xenon arc (XBO 150 W) was used as light source. It was connected via a light guide (spectral range, 400–800 nm; Schölly) to a perimeter (50 cm in diameter) placed around the animal. Either a linear polarizer (HN38S; Polaroid) or a neutral density filter of equal transmission to present unpolarized light was moved into the light path (irradiance, 105 $\mu W/cm^2$; angular size, 3°). The polarizer was rotated via custom-built hardware and software by 360° at speeds between 15 and 60°/s. To analyze rotation-specific components of the response that might result from latency effects, equal numbers of clockwise and counterclockwise rotations of the polarizer were tested during each recording. An *E*-vector orientation parallel to the longitudinal axis of the animal was defined as 0°. To investigate the bilateral extent of the receptive fields of the recorded neurons, the polarizer was presented from different elevations along the right–left meridian, covering a range from 0° elevation on either side of the animal up to 90° elevation (zenith).

In addition, a moving grating was presented in front of the locust. It consisted of a piece of cardboard (70° × 120°) with alternating black and white bars (70° × 10°). It was moved by hand in front of the animal from right to left and vice versa, resulting in a contrast frequency of ~3 Hz.

Data analysis. Sampled spike trains were stored on a computer and evaluated using Spike2 software (Cambridge Electronic Design) with implemented, custom-designed scripts. Action potentials were detected with threshold-based event detection. By using a gliding average algorithm at a bin size of 1 s, the detected events were converted into a mean frequency. Mean background activities during darkness were obtained from counts of spikes in a defined time interval (usually 12 s) before and between visual stimuli. Neuronal responses to polarized light were analyzed using Oriana 2.02a (Kovach Computing Services) for circular statistics and Origin 6.0 (Microcal) for curve fitting. Events within each 360° rotation of the polarizer were assigned a corresponding *E*-vector angle to quantify responses to polarized light. A list of these angles was exported for each *E*-vector rotation, and all individual and combined rotations of each neuron were tested statistically for polarization sensitivity. If the distribution of these angles during *E*-vector rotation was significantly different from randomness (Rayleigh's test for axial data), a neuron was rated polarization sensitive. The mean angle of the distribution was defined as the Φ_{max} value of that neuron. Differences in Φ_{max} values of clockwise and counterclockwise rotations ($\Delta\Phi_{max}$) were statistically analyzed with Student's *t* test for paired samples using SPSS software (version 11.5; significance level, 0.05), after the data were tested for normal distribution using the Kolmogorov–Smirnov test (significance level, 0.05). For illustration of *E*-vector tuning characteristics, mean activities from all polarizer rotations from neurons of the same type were plotted after normalization against background activity and adjustment to identical Φ_{max} at 0°.

To calculate the amplitude of frequency modulation and thus the strength of a polarized-light response (response amplitude *R*), each filter rotation was divided into 20° bins. The spiking frequency within each bin was calculated, as well as the mean frequency over all bins. The summed, absolute difference between the mean frequency and the individual frequencies was defined as the *R* value of that polarized-light response. *R* values derived from rotations at different rotation velocities were directly comparable, because we used instantaneous spike rate as a measure of neural activity rather than spike counts per bin (Labhart, 1996; Pfeiffer, 2006). To quantify background variability, the *R* value of a spike train during periods when no stimulus was applied was calculated and normalized to the mean response amplitude of that neuron. The resulting values indicate how much of the response amplitude during stimulation was attributable to background variability.

To investigate the bilateral extent of the receptive fields, response amplitudes (*R* values) were calculated for stimuli at different elevations along the right–left meridian. For each neuron, *R* values were normalized with respect to the maximum response amplitude and plotted against elevation. The mean lateral extent of the receptive field of a neuron type was established by averaging the means from all recorded neurons at each elevation.

For estimation of daytime relations, the preferred *E*-vector orientations were plotted against time of recording. Linear regression and correlation analysis were performed in Origin 6.0 software. The correlation coefficient (R_{cor}) was calculated, and a significant difference from a zero-slope regression was tested by applying Student's *t* test (significance level, 0.05). All circular plots and plots shown in Figures 4 and 6 were created using Origin 6.0 (Microcal).

Histology. After recording, the thoracic cavity was rinsed with locust saline, and the window in the pronotum was sealed with a piece of tissue. The locust was incubated overnight in a moist chamber at 4°C to allow diffusion of the tracer. On the next day, the brain and ventral nerve cord without the free abdominal ganglia were dissected out and fixed in a mixture of 4% paraformaldehyde, 0.25% glutaraldehyde, and 2% saturated picric acid (in 0.1 M phosphate buffer) overnight at 4°C. Ganglia were processed as whole mounts. They were rinsed four times for 15 min in PBS, dehydrated through an increasing ethanol series (25, 50, 70, 90, 95, and 100%; 15 min each), transferred to a 1:1 mixture of ethanol and methylsalicylate for 15 min, and, finally, cleared in methylsalicylate for at least 45 min. When Neurobiotin was injected into the neurons, ganglia were incubated with cyanine 3-conjugated streptavidin (1:1000; Dianova) for 3 d at 4°C in PBT (PBS including 0.5% Triton X-100), followed by rinsing with PBT (three times for 10 min) and PBS (six times for 30 min). Ganglia were finally mounted in Permount (Thermo Fisher Scientific) between two coverslips. Adhesive strips were used as spacers to avoid compressions. Neurons were scanned with a confocal microscope (Leica TCS-SP2) equipped with a 10× oil-immersion objective (HC PL APO 10×/0.4 Imm Corr CS) at minimal pinhole size and intervals of 4 μm. Reconstructions based on the data stacks were performed using Adobe Photoshop CS2.

To acquire higher morphological resolution of Neurobiotin-injected neurons, some ganglia were rehydrated and embedded in albumin–gelatin (4.8% gelatin and 12% ovalbumin in demineralized water) for sectioning. Embedded ganglia were postfixed in 8% formaldehyde (in 0.1 M

phosphate buffer) overnight at 4°C. Using a vibrating blade microtome (VT 1200S; Leica), the ganglia were sectioned in thick sections (130 μm thickness) (for details, see Heinze and Homberg, 2008). These preparations were scanned at high resolution (40× or 63× objective, HCX PL Apo 40×/1.25 oil or HCX PL Apo 63×/1.32 oil) and are shown as maximum intensity projections or as single optical sections. All images were optimized for contrast and brightness and described corresponding to the body axis.

The rehydrated preparations were also used for immunofluorescent colabeling with antibodies against GABA, serotonin, locustatachykinin II, A-type allatostatin, FMRFamide, or pigment-dispersing hormone, and against synapsin. For the detailed protocol and specificity of synapsin and serotonin immunostaining, see Heinze and Homberg (2008). The anti-GABA antibody (NT-108; Protos Biotech Corp.) was raised in guinea pig. It was used at a dilution of 1:500. The anti-locustatachykinin II (Lom-TK II) antiserum (K1-50820091) was donated by Dr. Hans Agricola (University of Jena, Jena, Germany) and was used at a dilution of 1:30,000. Its specificity on *S. gregaria* brain sections has been characterized by Vitzthum and Homberg (1998). For staining of neurons containing A-type allatostatins (AST-A), an antiserum against *Diploptera punctata* allatostatin 7 was used. The antiserum was a gift from Dr. Hans Agricola and was used at a dilution of 1:15,000. Competitive ELISA showed that the serum cross-reacts with other members of the A-type allatostatin family of peptides with a common Y/FXFGLamide C terminus (Vitzthum et al., 1996). The anti-FMRFamide antiserum (#671, used at 1:4,000) was generated against synthetic FMRFamide conjugated to thyroglobulin (Marder et al., 1987) and was generously supplied by Dr. Eve Marder (Brandeis University, Waltham, MA). Specificity tests by radioimmunoassay showed cross-reactivity of the antiserum with various C-terminally extended MRFamides and LRFamides (Marder et al., 1987). The anti-pigment-dispersing hormone (PDH) serum (#3B3, used at dilutions of 1:20,000) was raised in rabbit against conjugates of synthetic *Uca pugilator/Cancer magister* β-PDH and bovine thyroglobulin. Its specificity was demonstrated by Dircksen et al. (1987) and Homberg et al. (1991).

Results

Descending POL-neurons in the locust nervous system

Through intracellular recordings combined with dye fills, we identified three types of descending POL-neurons in the nervous system of the desert locust. In total, 26 intracellular recordings were obtained from axons in the neck connectives or from neuronal processes in the posterior protocerebrum of the brain. Dye injections were successful in 17 neurons, belonging to three morphological types. Nine neurons that could not be stained were assigned to the three types based on their physiological response properties. Two of the three neuron types had descending axons from the brain, one descended through the ipsilateral and the other through the contralateral connective. The third type had no arborizations in the brain but was a contralaterally descending neuron from SOG. In some preparations, more than one cell was stained. In these cases, one of the neurons, interpreted as the recorded cell, was stained more intensely, whereas others appeared less strongly fluorescent. The most likely reason for these colabelings is dye leakage through injury of neighboring axons.

The responses of the descending neurons to polarized light were highly variable. In some recordings, the responsiveness varied in relation to arousal of the animal, characterized by spontaneous activity bursts of the animal correlated with high spiking frequency of the recorded neuron; a previously quiescent animal suddenly began a series of vigorous movements that quickly subsided, leaving the animal as quiet as before. In other recordings, spontaneous activity changes of the recorded neuron occurred without observable movements of the animal. In some cases, neural activity changes were correlated with stimulus presentation, but in most cases, they occurred apparently independent of visual input. Changes in arousal or spontaneous activity often corresponded with shifts in baseline and usually affected the responsiveness of the neurons. In extreme cases, neurons switched from highly polarization-sensitive to polarization blind after a change in background activity and baseline. Spike traces during *E*-vector rotations that were accompanied by increased arousal, as indicated by movements of legs, wings, or antenna, were therefore not included in the analysis. Similar variability in responsiveness has also been observed in other locust visual interneurons and was particularly noted for the descending deviation detector interneuron with input from the contralateral ocellus (Kien, 1976; Rowell and Reichert, 1986). In the central complex, certain cell types were, likewise, highly polarization sensitive in some recordings but polarization blind in others (Heinze and Homberg, 2009). Release of the neuromodulator octopamine has been proposed frequently to affect state-dependent sensory responsiveness and arousal in insects (Bacon et al., 1995; Longden and Krapp, 2009) and may possibly underlie the effects seen here.

Ipsilaterally descending brain neurons

Stable recordings from ipsilaterally descending POL-neurons were obtained in six experiments with successful staining in three cases. The morphologies of the stained neurons were indistinguishable, suggesting that all recordings were from the same neuron. Their somata were located near the posterior brain surface medioventrally from the calyces of the mushroom body (Fig. 1*A*). Fine and, therefore probably dendritic, arborizations were concentrated in the posterior protocerebrum near but not within the posterior optic tubercle (Fig. 1*G*) and close to the posterior surface of the brain. Beaded ramifications, suggesting neuronal output regions (Strausfeld, 1976; Peters et al., 1986), occurred in the antennal mechanosensory and motor center (Fig. 1*H*). An axonal fiber descended through the ipsilateral connective into the SOG and all thoracic ganglia and terminated with a few small side branches in the metathoracic ganglion. Arborizations in the SOG and prothoracic ganglion had bleb-like and, therefore presumably presynaptic, endings (Strausfeld, 1976) in dorsal parts of the ganglia. All arborizations were restricted to the ipsilateral hemispheres of the ganglia.

The ipsilaterally descending neurons ($n = 6$) had highly variable background activity ranging from <1 spike per second up to 47 impulses per second (mean ± SE, 17.8 ± 6.8 impulses per second). All neurons showed polarization opponency (Fig. 1*B*,*C*), i.e., they were maximally excited by a particular *E*-vector (Φ_{max}) and were maximally inhibited by an *E*-vector perpendicular to Φ_{max}. This is particularly obvious when plotting normalized mean activities of the six neurons for all polarizer rotations after adjustment to identical Φ_{max} (Fig. 1*D*). Corresponding to the large variation in background activity (background variability, 64 ± 12.1%), the activity during stimulation with polarized light was also highly variable ($r = 78.2 \pm 16.6$). The preferred *E*-vector orientations (Φ_{max}) were higher during counterclockwise rotations of the polarizer than during clockwise rotations ($\Delta\Phi_{max} = 36.3° \pm 13.0°$, mean ± SD, $n = 6$ neurons). The average Φ_{max} orientations calculated from equal numbers of clockwise and counterclockwise rotations of the polarizer were 14°, 149°, and 176° (data not shown) and 128° (Fig. 1) for four neurons with somata in the left brain hemisphere and 36° and 70° for two neurons with somata in the right brain hemisphere (data not shown). In one recording (data not shown), we measured the polarization tuning along the right–left meridian over a range of 180° and found the neurons sensitivity to polarized light to fully extend into the ipsilateral and contralateral visual field. One neuron, recorded in the left hemisphere, was tested for motion sen-

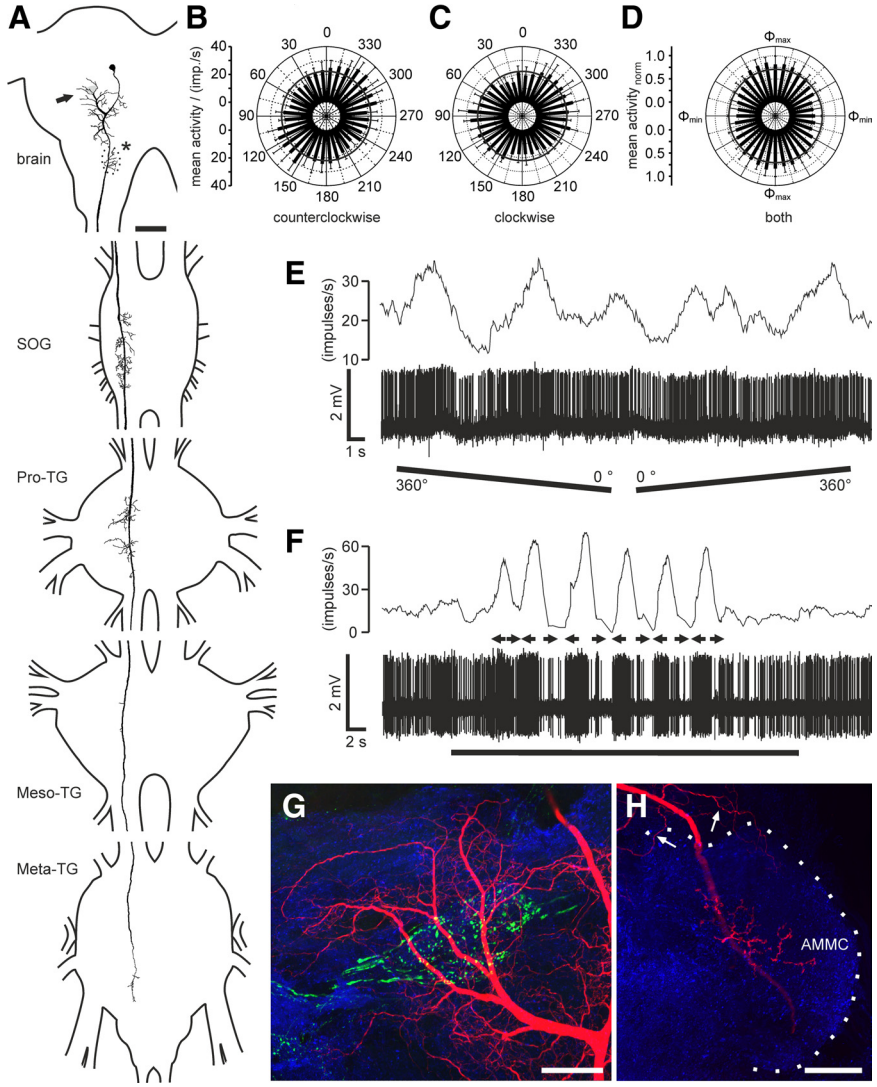

Figure 1. Morphology and response characteristics of ipsilaterally descending brain neurons. ***A***, Reconstruction of arborizations in the brain (posterior view), SOG, and the three thoracic ganglia (dorsal view). Arborizations in all ganglia are confined to the ipsilateral hemispheres. Dendritic ramifications are in the posterior protocerebrum at the level of the posterior optic tubercle (arrow; POTu, gray shaded; see also ***G***). The antennal mechanosensory and motor center (dotted line, asterisk; see also ***H***) is invaded by beaded arborizations. An axonal fiber descends through the SOG with ramifications extending laterally and medially around the axon. In the Pro-TG, two characteristic areas of ramification extend laterally. The axon passes through the mesothoracic (Meso-TG) and metathoracic (Meta-TG) ganglion, with only sparse side branches, and could not be traced beyond the fused first abdominal ganglion. ***B***, ***C***, Circular diagrams of mean frequencies of action potentials plotted against *E*-vector orientation during dorsal stimulation with a rotating polarizer. Background activity is indicated by a black circle within each plot. ***B***, During counterclockwise rotations of the polarizer, *E*-vector tuning (Φ_{max}) was at 142° ($n = 7$; error bars indicate SD; bin size, 10°; $p = 1.9 \times 10^{-12}$). ***C***, The preferred *E*-vector orientation during clockwise rotations ($n = 7$; error bars indicate SD; bin size, 10°; $p = 2.2 \times 10^{-8}$) had a Φ_{max} of 111° and differed significantly from Φ_{max} during counterclockwise rotations ($n = 7$; $p = 0.009$, Student's *t* test for paired probes). ***D***, Circular diagram showing normalized mean activities from all recordings ($n = 6$) to dorsal stimulation through a rotating polarizer with Φ_{max} set to 0°. Background activity is indicated by a black circle. ***E***, Spike train (bottom trace) and mean spiking frequency (top trace; gliding average with bin size of 1 s) from the same neuron as in ***B*** and ***C*** during a counterclockwise (360–0°) and a clockwise (0–360°) rotation of the polarizer. ***F***, Responses to a moving black and white grating presented in front of the animal. A small cardboard with black and white stripes was moved by hand from left to right and vice versa under unpolarized light condition (black bar). Black arrows indicate movement direction of the pattern as seen by the locust. The neuron with the soma in the left brain hemisphere was excited by movement from right to left and shows inhibition to moving bars from left to right. ***G***, ***H***, Morphological details in the brain. Maximum intensity views of optical sections (frontal plane; thickness, 2 μm) from confocal image stacks showing anti-synapsin staining (blue), anti-PDH immunostaining (green), and ramifications of the Neurobiotin-stained neuron (red). ***G***, Maximum intensity projection of 78 optical sections showing ramifications around the posterior optic tubercle (POTu), which is marked with the anti-PDH antiserum. ***H***, Maximum intensity projection of two combined stacks (76 optical sections), showing varicose arborizations in the antennal mechanosensory and motor center (AMMC). Some dendritic arborizations are visible dorsally from the antennal mechanosensory and motor center. Scale bars: ***A***, 200 μm; ***G***, ***H***, 40 μm.

sitivity. The neuron was highly excited by the grating moving from right to left in front of the animal but remained silent during movement in the opposite direction (Fig. 1*F*).

Contralaterally descending brain neurons

Four contralaterally descending POL-neurons were recorded and stained. Again, the morphologies of the neurons were indistinguishable, suggesting that recordings were from the same neuron. Their cell bodies were located in the posterior median pars intercerebralis at the level of the central body (Fig. 2*A*). Protocerebral ramifications were concentrated in the posterior protocerebrum near the posterior surface of the neuropil. The main axonal fiber crossed the midline and descended through the contralateral connective to the SOG, all thoracic ganglia, and to the free abdominal ganglia, but their projections in the abdominal ganglia could not be revealed. Terminals in the SOG and Pro-TG had a bleb-like structure, suggesting output sites, and beaded endings were also found in the contralateral antennal mechanosensory and motor center in the brain. One neuron was recorded from the left connective and had its soma in the right brain hemisphere. The other three neurons were recorded from the input regions in the left brain hemisphere and descended through the right connective.

Responses of the contralaterally descending neurons ($n = 4$) to polarized light were weak compared with those of the ipsilaterally descending neurons and did not show large interindividual differences in response amplitude ($r = 38.3 \pm 11.8$). The average response of normalized mean activities, nevertheless, shows clear *E*-vector tuning, but without polarization opponency (Fig. 2*D*). The background activity varied between 0.6 and 16 impulses per second (3.5 ± 1.2 impulses per second; $n = 4$). The variability in background spiking activity was 45% ($n = 1$). It could not be calculated for the other three neurons because of lack of recording intervals without visual stimulation. As found for the ipsilaterally descending neurons, the neurons showed higher Φ_{max} values during counterclockwise rotations of the polarizer than during clockwise rotations ($\Delta\Phi_{max} = 41.3° \pm 12.7°$, mean ± SD, $n = 2$). Average preferred *E*-vector orientations (Φ_{max}) calculated from clockwise and counterclockwise rotations were at 70°, 87°, and 102° (data not shown) for the three neurons descending through the right connective and

130° (Fig. 2) for the fourth neuron descending through the left connective. Motion stimuli were tested in one recording. The neuron showed strong responses with activation to moving black and white bars in front of the animal from left to right and vice versa (Fig. 2*F*). The motion response showed considerable adaptation.

SOG neurons

Neurons descending from the SOG were recorded in 16 experiments. Ten of these neurons were labeled. The somata of the stained neurons were located anterolaterally in the labial neuromere. Their arborizations in the SOG were restricted to a small tree lateral to the ipsilateral dorsal intermediate tract and beaded contralateral branches leaving the axon and arborizing in the labial neuromere dorsal and lateral to the dorsal intermediate and ventral lateral tract. Neurons of this type had been described by Kien et al. (1990) as a cluster of three neurons. Their cell bodies, arborizations, and axons lie closely together at the labial–maxillary junction in the SOG, and at least one, but more likely two, of the axons terminate in the Pro-TG (Kien et al., 1990). The descending POL-neurons stained here (Fig. 3*D*) shared all morphological features within the SOG with the neurons described by Kien et al. (1990). All neurons ramified with beaded endings in a narrow area of the contralateral Pro-TG close to the dorsal neuropil surface.

The descending SOG neurons responded with polarization opponency to dorsally presented polarized light, illustrated by the spindle-shaped circular plot of the normalized mean activities of rotations from the 16 recordings (Fig. 3*C*). The neurons had a mean background activity of 4.9 ± 1.4 impulses per second ($n = 15$). Most SOG neurons showed strong modulation during stimulation with a rotating polarizer ($r = 57.0 \pm 4.9$). They were activated up to peak frequencies of 20.2 ± 8.3 impulses per second at Φ_{max} and were usually totally silenced at Φ_{min} (Fig. 3*A*,*B*,*E*). The background variability of these neurons was similar to that of the ipsilaterally descending neurons (61 ± 7.2%). The ratio of response amplitude versus firing rate was clustered rather than linearly correlated (data not shown). Φ_{max} values ranged from 3° to 137° and covered three-quarters of the total possible range of *E*-vectors (see Fig. 6*C*). The Φ_{max} distribution appeared to be clustered around 42° and 116° but was not significantly different from randomness (Rao's spacing test, $p > 0.1$). Like the descending brain neurons, the SOG neurons showed higher Φ_{max} values during counterclockwise rotations of the polarizer than during clockwise rotations (Fig. 3). The $\Delta\Phi_{max}$ values of the SOG neurons (48.4° ± 7.4°, $n = 15$) differed significantly from those of the two brain neurons ($p = 0.014$, one-way ANOVA).

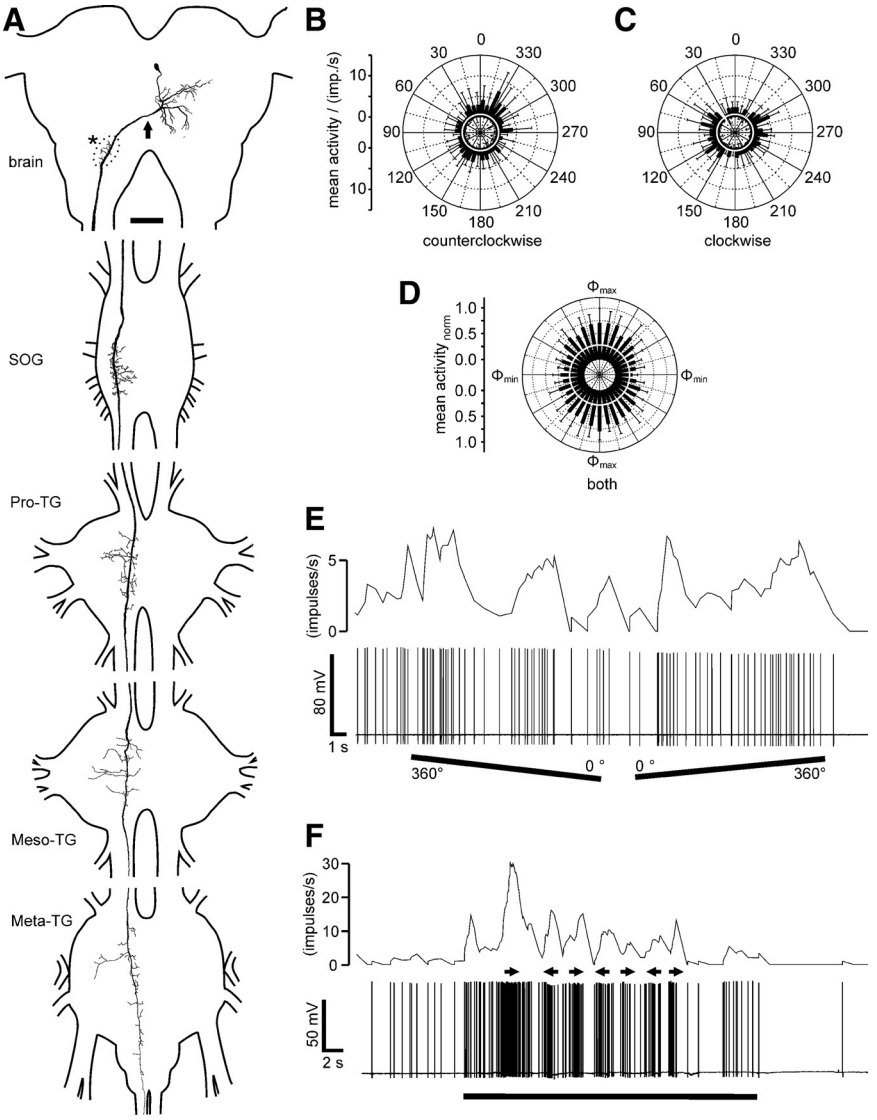

Figure 2. Morphology and response characteristics of a contralaterally descending brain neuron (***A–C***, ***E***, ***F***) and normalized average response of all recordings (***D***). ***A***, Reconstruction of arborizations in the brain (posterior view), SOG, and the three thoracic ganglia (dorsal view). The neuron has its soma and presumably dendritic arborizations in the ipsilateral posterior median protocerebrum. The axon crosses the midline of the brain (arrow) and descends through the contralateral connective. Presumably presynaptic endings with beaded terminals are in the antennal mechanosensory and motor center (asterisk). The neuron descends through the SOG and thoracic ganglia and sends a fiber, which could not be traced further, into the connective toward the free unfused abdominal ganglia. All ramifications in the ventral nerve cord are confined to the contralateral hemisphere and have beaded, presumably presynaptic, terminals in dorsal aspects of the ganglia. Meso-TG, Mesothoracic ganglion; Meta-TG, metathoracic ganglion ***B***, ***C***, Circular diagrams of mean frequencies of action potentials of the neuron against *E*-vector orientation during dorsal stimulation with a rotating polarizer. Each rotation direction is shown separately. Background activity is indicated by a white circle within each plot. ***B***, During counterclockwise rotations of the polarizer, the neuron had a preferred *E*-vector orientation (Φ_{max}) of 157° ($n = 5$; error bars indicate SD; bin size, 10°; $p = 7.38 \times 10^{-4}$). ***C***, The preferred *E*-vector orientation during clockwise rotations ($n = 5$; error bars indicate SD; bin size, 10°; $p = 5.74 \times 10^{-4}$) had a Φ_{max} of 103° and differed significantly from Φ_{max} during counterclockwise rotations ($n = 5$; $p = 0.002$, Student's *t* test for paired probes). ***D***, Circular diagram showing normalized mean activities from all recordings ($n = 4$) to dorsal stimulation through a rotating polarizer with Φ_{max} set to 0°. Background activity is indicated by a white circle. ***E***, Spike train (bottom trace) and mean spiking frequency (top trace; gliding average with bin size of 1 s) of the neuron during a counterclockwise (360–0°) and a clockwise (0–360°) rotation of the polarizer. ***F***, Responses to a moving black and white grating presented in front of the animal. A small cardboard with black and white stripes was moved by hand from left to right and vice versa under unpolarized light condition (black bar). Black arrows indicate movement direction of the pattern as seen by the locust. The neuron was activated during movements in both directions. The response decreased with repetition of stimuli. Scale bar, 200 μm.

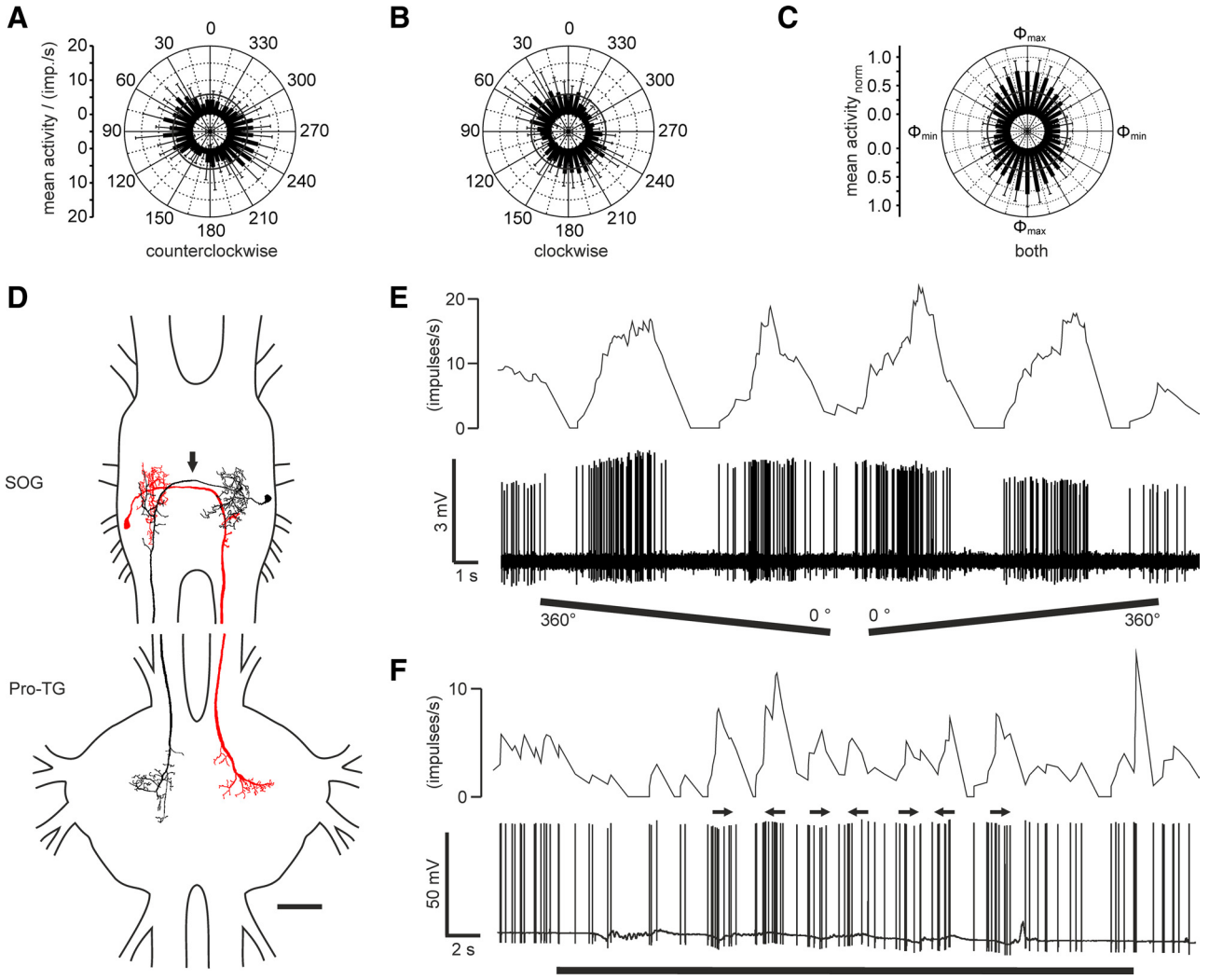

Figure 3. Response characteristics and morphology of descending neurons from the SOG. ***A***, ***B***, Circular diagrams of mean frequencies of action potentials of the neuron against *E*-vector orientation during dorsal stimulation with a rotating polarizer. Each rotation direction is shown separately. Background activity is indicated by a black circle within each plot. ***A***, During counterclockwise rotations of the polarizer, the neuron had a preferred *E*-vector orientation (Φ_{max}) of 70° ($n = 11$; error bars indicate SD; bin size, 10°; $p < 10^{-12}$). ***B***, The preferred *E*-vector orientation (Φ_{max}) during clockwise rotations ($n = 11$; error bars indicate SD; bin size, 10°; $p < 10^{-12}$) was at 27° and differed significantly from Φ_{max} during counterclockwise rotations ($n = 11$; $p < 0.001$, Student's *t* test for paired probes). ***C***, Circular diagram showing normalized mean activities from all recordings ($n = 16$) to dorsal stimulation through a rotating polarizer with Φ_{max} set to 0°. Background activity is indicated by a black circle. ***D***, Horizontal superimposed reconstructions (dorsal view). The red neuron is mirrored. Both neurons differ slightly in morphology. They have their somata and presumably dendritic arborizations in posterior parts in the ipsilateral hemisphere of the SOG. Axons cross the midline (arrow), give rise to presumably presynaptic endings with bleb-like structures that partly overlap with the input region of the contralateral homolog, and descend through the contralateral connective. The neurons have axonal beaded ramifications that differ slightly between the two cells in a narrow dorsal part of the Pro-TG. ***E***, Spike train (bottom trace) and mean spiking frequency (top trace; gliding average with bin size of 1 s) of the same neuron as in ***A*** and ***B*** during a counterclockwise (360 – 0°) and a clockwise (0 – 360°) rotation of the polarizer. ***F***, Responses to a moving black and white grating presented in front of the animal (red neuron in ***D***). A small cardboard with black and white stripes was moved by hand from left to right and vice versa under unpolarized light condition (black bar). Black arrows indicate movement direction of the pattern as seen by the locust. The neuron showed weak activations to movements in both directions. Scale bar, 200 μm.

Eight neurons were tested for motion sensitivity but showed only weak bidirectional responses to the moving grating (Fig. 3*F*). Polarization tuning along the right–left meridian was tested in 10 recordings (Fig. 4*A*). The response strength to laterally presented polarized light (0° elevation) was as strong as the response to zenithal stimulation (90°), and all neurons were polarization sensitive over the tested range of 180° along the right–left meridian (Fig. 4*B*). In these neurons, Φ_{max} increased significantly when moving the polarizer from ipsilateral positions to positions in the contralateral hemisphere ($R_{cor} = 0.53$; *t* test against the slope of zero, $p = 0.00453$) (Fig. 4*C*).

The SOG neurons showed no colabeling with antisera against the inhibitory neurotransmitter GABA, serotonin, and the neuropeptides FMRFamide, Lom-TK II, and allatostatin-A, indicating that the neurons use a neurotransmitter/modulator different from the immunocytochemically tested substances (Fig. 5).

Distribution and daytime dependence of Φ_{max} orientations

Judged by the striking morphological similarity in all stained preparations, the ipsilaterally and contralaterally descending POL-neurons from the brain probably exist only once per hemisphere. Φ_{max} values calculated from the different recordings from descending brain neurons covered the full 180° range of possible *E*-vectors (data not shown; Rao's spacing test, $p > 0.95$). When neurons with axons in the left (Fig. 6*A*) and right (Fig. 6*B*) connective were plotted separately, Φ_{max} distributions appeared to be clustered around 154° (Fig. 6*A*, left connective) and 74° (Fig. 6*B*, right connective) respectively, but in both cases, the distributions were not significantly dif-

ferent from randomness (Rao's spacing test, $p > 0.1$). Likewise, when Φ_{max} orientations from ipsilaterally and contralaterally descending neurons were analyzed separately, the distributions were not significantly different from randomness either (Rao's spacing test, $p > 0.1$; data not shown).

All recordings were performed between 9:00 A.M. and 6:00 P.M. (Central European Time). Figure 7 shows the Φ_{max} values of all recordings in relation to the time of recording. A linear correlation exists between the time of recording and *E*-vector tuning (Φ_{max}) for the descending neurons from the brain if considered as a functional unit of ipsilaterally and contralaterally descending POL-neurons ($R_{cor} = -0.9$, *t* test against the slope of zero, $p = 0.00039$) (Fig. 7*A*). The slope of the regression line indicates a shift in Φ_{max} tuning of 21.5°/h, covering 516° in 24 h. No correlation between daytime and *E*-vector tuning was found in the SOG neurons ($R_{cor} = 0.11$, $p = 0.97$) (Fig. 7*B*).

Discussion

We have characterized three types of descending neuron in the desert locust that are sensitive to the *E*-vector orientation of dorsally presented polarized light. Based on morphological similarities, we suggest that the recordings were from two bilateral pairs of descending brain neurons, one with ipsilaterally and the other with contralaterally descending axon, and from two bilateral pairs of descending SOG neurons. Additional POL-neurons may exist but were not encountered. Given the established role of dorsal eye regions in detecting the polarization pattern of the sky (Labhart and Meyer, 1999), the neurons are likely to be involved in behavioral responses to sky polarization such as sky compass orientation. The ipsilaterally descending neuron and the SOG neurons showed polarization opponency. The polarization tuning through a range of up to 180° along the right–left meridian and the high background variability of the neurons continue trends in the central-complex network toward increasing receptive field size and decreasing signal-to-noise ratio (Heinze et al., 2009), suggesting that the neurons are at a later stage of processing than the outputs of the central complex. All neurons were multisensory and responded, in addition, to horizontal motion along the eye equator in the frontal to frontolateral visual field.

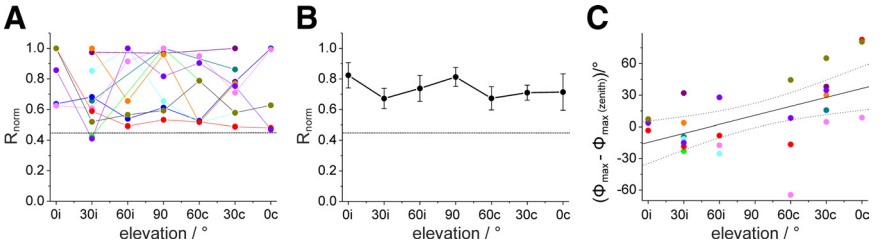

Figure 4. Polarized-light sensitivity and *E*-vector tuning of the descending SOG neurons when stimulated with polarized light from different elevations along the right–left meridian. ***A***, Response amplitudes from individual recordings, distinguished by different colors, plotted against elevation of polarized-light stimulus. Elevation is plotted with respect to the location of the soma (0i–60i in the ipsilateral and 0c–60c in the contralateral hemisphere of the SOG) and was sampled along the right–left meridian with respect to the locust. Values were normalized to the largest *R* value of each neuron (i.e., the receptive field center). Data points are connected by lines for better visibility. Dotted line indicates background variability for the neuron type, which has been renormalized with respect to the mean receptive field center. ***B***, Average receptive field for the examined SOG neurons. Dotted line, Background variability. Values are means ± SE. ***C***, Deviations of Φ_{max} values at different elevations from zenithal Φ_{max} values. Differences in Φ_{max} values are plotted against the elevation. A significant correlation was observed ($R_{cor} = 0.53$, $p = 0.00453$). Colors of data points correspond to the colors in ***A***.

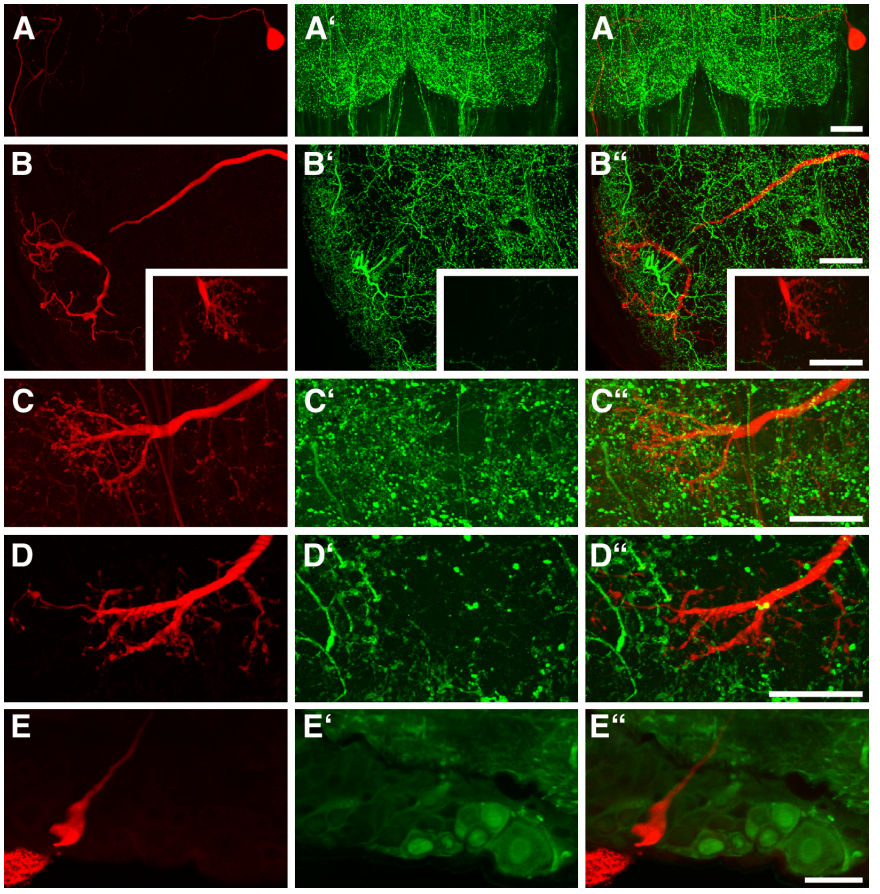

Figure 5. Confocal images of 130 μm sections showing parts of Neurobiotin-stained descending SOG neurons (red) combined with immunostaining using antisera against FMRFamide, serotonin, Lom-TK II, AST-A, or GABA (green). The Neurobiotin-stained somata and ramifications are shown in ***A–E***, the immunostainings are shown in ***A′–E′***, and the combined illustrations are shown in ***A‴–E‴***. None of the tested neuroactive substance is localized in the stained neurons. ***A***, Soma and part of the primary neurite in the SOG. FMRFamide immunostaining is not present in the soma or axon of the neuron. ***B***, Dendritic ramifications in the SOG and presynaptic terminals from the Pro-TG (inset). The labeled neuron does not show serotonin immunostaining. ***C***, ***D***, In the Pro-TG, presynaptic terminals with bleb-like endings do not show immunostaining for Lom-TK II (***C***) or AST-A (***D***). ***E***, The soma of the SOG neuron does not exhibit GABA immunostaining. Scale bars, 40 μm.

POL-neurons descending from the brain

Both brain neurons responded with sinusoidal activity changes to a rotating polarizer. Whereas the ipsilaterally descending neuron showed considerable variations in the responses, the contralaterally descending neuron in general had lower background activity and responded less strongly to polarized light. Both descending neurons were strongly driven by horizontal motion presented in

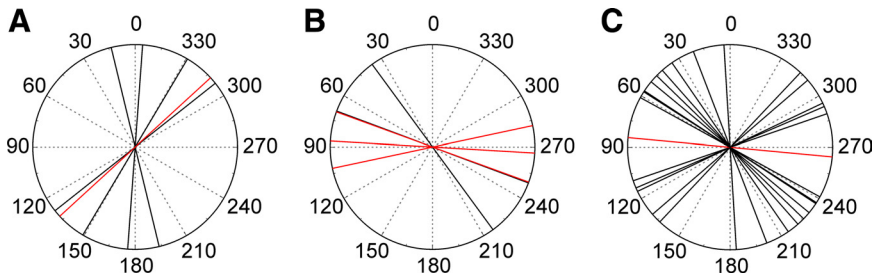

Figure 6. Distribution of Φ_{max} values in the three types of descending neuron. ***A***, Φ_{max} values from brain POL-neurons with descending axons in the left connective. *E*-vector orientations (ipsilaterally descending, black; contralaterally descending, red) seem to be clustered around 154°, but the distribution is not significantly different from randomness (Rao's spacing test, $p > 0.01$). ***B***, Φ_{max} values from brain POL-neurons with descending axons in the right connective. Φ_{max} values are clustered around 74°, but the distribution is not significantly different from randomness (Rao's spacing test, $p > 0.1$; same color code as in ***A***). ***C***, Φ_{max} values of all SOG neurons (the red value is mirrored) descending through the left connective. Φ_{max} values are clustered around 42° and 116°, but the distribution is not significantly different from randomness (Rao's spacing test, $p > 0.1$).

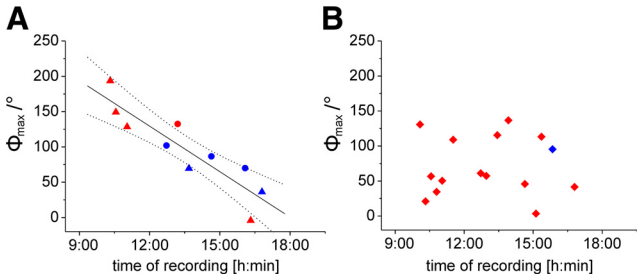

Figure 7. Daytime-dependent preferred *E*-vector orientations (Φ_{max}) in descending POL-neurons. Φ_{max} values of the three descending neuron types are plotted against standard time (Central European Time) of recording. ***A***, A correlation was observed for the combined values from the two types of brain descending neuron ($R_{cor} = -0.9$, *t* test against the slope of 0, $p = 0.00039$; $y = -515.91x + 387.37$), indicated by the regression line with 95% confidence intervals. Data from ipsilaterally descending neurons (triangles) and contralaterally descending neurons (dots) are included. Neurons with axons in the left connective are shown in red and those with axons in the right connective in blue. ***B***, No correlation was observed for the descending SOG neurons ($R_{corr} = 0.11$, $p = 0.97$). Most SOG neurons were recorded from the left connective (red squares); only one recording was from the right connective (blue square).

the frontal visual field. The ipsilaterally descending brain neuron has remarkable anatomical and physiological similarities with the descending direction-selective motion-detecting neuron (PDDSMD neuron) (Rind, 1990). The PDDSMD neuron is sensitive to motion stimuli signaling yaw deviations as suggested by directional preferences for front-to-back motion across the ipsilateral and back-to-front motion across the contralateral eye, respectively. Correspondingly, the ipsilaterally descending neuron studied here was excited by horizontal motion in front of the animal only when movement occurred toward the ipsilateral but not toward the contralateral eye. The contralaterally descending POL-neuron was described by Williams (1975) as one of a pair of neurons with somata in the pars intercerebralis termed PI(2):5 and PI(2):6. In contrast to the PI(2):5 neuron, PI(2):6, recorded here, has no processes extending to the lateral ocellar tract and a less pronounced anteroventral branch. Both neurons share extensive superficial arborizations in the posteroventral brain (Williams, 1975). The PI(2):5 neuron was physiologically characterized as one of several descending deviation detector neurons in flying locusts (Hensler, 1988; Hensler and Rowell, 1990), but PI(2):6 has not been studied physiologically before.

The two descending brain neurons characterized here extend the hitherto known polarization vision pathway from the brain to thoracic motor circuits. Judged by their ramifications in the posterior protocerebrum, both neurons might receive polarization-sensitive input from the LAL–pPC neuron described by Heinze and Homberg (2009). The LAL-pPC neuron receives input in the lateral accessory lobe (LAL) and gives rise to bilaterally symmetric output ramifications in the posterior protocerebrum (pPC). Therefore, the ipsilaterally and contralaterally descending POL-neurons might receive identical polarized-light input signals. Additionally, both neurons are sensitive to horizontal motion. In free flight, changes in yaw would create both a polarization signal from the sky and a yaw motion signal from the surrounding landscape. Both signals apparently converge on the brain descending neurons studied here and might result in robust coding of changes in head orientation under various sky and ground contrasts. Testing both stimulus modalities in the same recording will show how both inputs exactly interact and complement each other.

The putative output ramifications of the descending POL-neurons are concentrated in dorsal parts of the thoracic ganglia in which thoracic motor neurons receive their input (Siegler et al., 1991; Schlurmann and Hausen, 2007). Hence, the descending POL-neurons are likely to provide direct input to thoracic motor centers and might be the final interneurons of the polarization vision pathway from the receptor cells in the dorsal rim area of the eye to motor neurons controlling gaze, gate, and flight.

Polarization vision and time compensation

A crucial requirement for a sky compass that controls migratory directions is to achieve time compensation, i.e., to continuously adjust the *E*-vector tuning of the neurons as the sun moves across the sky during the day. Because the polarization pattern of the blue sky is generated by sunlight, it moves across the sky during the day with an average change in solar azimuth of 15°/h. Time compensation accounting for this shift has been shown in behavioral experiments in honeybees, ants, and monarch butterflies (Lindauer, 1960; Wehner, 1992; Mouritsen and Frost, 2002; Reppert et al., 2010). Pfeiffer and Homberg (2007) suggested that a daytime-dependent compensation for changes in solar elevation operates in the anterior optic tubercle of the locust, an input stage to the central-complex network. How and at what stage of the polarization vision pathway solar azimuth compensation is achieved is currently unclear. El Jundi and Homberg (2010) provided evidence for the existence of a second polarization vision pathway in locusts that connects the accessory medulla to the central complex. In the fruit fly *Drosophila melanogaster* and the cockroach *Leucophaea maderae*, the accessory medulla is the site of the circadian clock controlling circadian changes in locomotion and other behaviors (Helfrich-Förster et al., 1998; Homberg et al., 2003, Helfrich-Förster, 2004), but whether this is also true for locusts remains to be seen.

The two descending brain neurons show *E*-vector tunings that are linearly correlated with time of day. Convergent information from the internal sky compass and the circadian clock therefore occurs in the brain at or upstream of the dendritic ramification of the descending neurons. For a compensation of solar azimuth changes, the Φ_{max} values of time-compensated POL-neurons should change by ~15°/h, which accounts for 360° azimuth changes in 24 h. The slope of the regression curve (21.5°/h) is close to this relation. Because all locusts used here were reared

under laboratory conditions, the diurnal shift in *E*-vector tuning we see might represent a default state that is determined genetically and might require environmental cues for adjustment to local sky conditions. The data implicate that, at any given daytime, the two pairs of descending neurons have the same *E*-vector tuning. This is at present difficult to explain, but again, *E*-vector tuning and daytime dependence may be strongly influenced by environmental conditions.

POL-neurons of the SOG

The descending POL-neurons of the SOG responded with polarization opponency to the rotating polarizer. The recordings did not provide evidence for time compensation and showed only weak unidirectional responses to moving stimuli. Based on Φ_{max} distribution (Fig. 6*C*), which shows two possible subclusters, the SOG neurons might consist of two bilateral pairs of neurons. This assumption is supported by Kien et al. (1990) who suggested a pair of these neurons per SOG hemisphere.

Hensler (1989) recorded from the neuron under tethered flying conditions. The neuron responded to simulated roll deviations and was rhythmically excited during flight. Electrical stimulation of the neuron resulted in head rolling to the contralateral side (Hensler, 1989). We therefore suggest that the SOG neurons do not take part in the polarization vision pathway used for navigation but may be involved in the control of flight stabilization as proposed by Hensler (1989). The neurons might integrate sky polarization input with horizon detection to control head orientation during flight, but how both inputs interact with each other in a biological meaningful way will have to be determined in future experiments.

Comparison to head direction cells

When stimulating with a rotating polarizer, shifts in Φ_{max} would be expected to account for differences in latencies of the response during clockwise and counterclockwise rotations. As a consequence of the delayed response to the preferred orientation, Φ_{max} should have higher values for clockwise and lower values for counterclockwise rotations. Furthermore, the $\Delta\Phi_{max}$ value should increase with increasing numbers of intercalated neurons between photoreceptors and the neuron of interest. Interestingly, however, Φ_{max} shifts in the opposite direction were observed. In all neurons, Φ_{max} values for counterclockwise rotations were higher than Φ_{max} values for clockwise rotations, and these differences were larger in the SOG than in the brain neurons. Similar shifts in directional tuning have been observed in head direction cells in the anterior dorsal thalamic nucleus and other areas involved in spatial orientation of rats (Blair and Sharp, 1995; Taube, 2007). Heinze and Homberg (2007) emphasized the similar biological roles of zenithal *E*-vector-coding neurons in locusts and head direction cells in rats for spatial orientation. Just as proposed for tuning shifts in head direction cells during clockwise and counterclockwise rotations of rats, the *E*-vector tuning shifts in POL-neurons observed here might signal anticipatory head direction in the near future (Blair and Sharp, 1995). At present, however, both the neural mechanisms and the functional roles underlying anticipatory firing of these neurons in rats are poorly understood (Taube, 2007). With recordings from identifiable neurons, the locust may be a good model to analyze the mechanisms and benefits of anticipatory head direction signaling in future experiments.

References

Bacon JP, Thompson KS, Stern M (1995) Identified octopamine neurons provide an arousal mechanism in the locust brain. J Neurophysiol 74:2739–2743.

Blair HT, Sharp PE (1995) Anticipatory head direction signals in anterior thalamus: evidence for a thalamocortical circuit that integrates angular head motion to compute head direction. J Neurosci 15:6260–6270.

Brunner D, Labhart T (1987) Behavioural evidence for polarization vision in crickets. Physiol Entomol 12:1–10.

Dacke M, Nordström P, Scholtz CH (2003) Twilight orientation to polarized light in the crepuscular dung beetle *Scarabaeus zambesianus.* J Exp Biol 206:1535–1543.

Dircksen H, Zahnow CA, Gaus G, Keller R, Rao KR, Riehm JP (1987) The ultrastructure of nerve endings containing pigment-dispersing hormone (PDH) in crustacean sinus glands: identification by an antiserum against a synthetic PDH. Cell Tissue Res 250:377–387.

El Jundi B, Homberg U (2010) Evidence for the possible existence of a second polarization-vision pathway in the locust brain. J Insect Physiol 56:971–979.

Fotowat H, Fayyazuddin A, Bellen HJ, Gabbiani F (2009) A novel neuronal pathway for visually guided escape in *Drosophila melanogaster.* J Neurophysiol 102:875–885.

Frye MA, Olberg RM (1995) Visual receptive field properties of feature detecting neurons in the dragonfly. J Comp Physiol A Neuroethol Sens Neural Behav Physiol 177:569–576.

Griss C, Rowell CHF (1986) Three descending interneurons reporting deviation from course in the locust. I. Anatomy. J Comp Physiol A Neuroethol Sens Neural Behav Physiol 158:765–774.

Heinze S, Homberg U (2007) Maplike representation of celestial *E*-vector orientations in the brain of an insect. Science 315:995–997.

Heinze S, Homberg U (2008) Neuroarchitecture of the central complex of the desert locust: intrinsic and columnar neurons. J Comp Neurol 511:454–478.

Heinze S, Homberg U (2009) Linking the input to the output: new sets of neurons complement the polarization vision network of the locust central complex. J Neurosci 29:4911–4921.

Heinze S, Gotthardt S, Homberg U (2009) Transformation of polarized light information in the central complex of the locust. J Neurosci 29:11783–11793.

Helfrich-Förster C (2004) The circadian clock in the brain: a structural and functional comparison between mammals and insects. J Comp Physiol A Neuroethol Sens Neural Behav Physiol 190:601–613.

Helfrich-Förster C, Stengl M, Homberg U (1998) Organization of the circadian system in insects. Chronobiol Int 15:567–594.

Hensler K (1988) The pars intercerebralis neurone PI(2)5 of locusts: convergent processing of inputs reporting head movements and deviations from straight flight. J Exp Biol 140:511–533.

Hensler K (1989) Corrective flight steering in locusts: convergence of extero- and proprioceptive inputs in descending deviation detectors. In: Neurobiology of sensory systems (Singh RN, Strausfeld NJ, eds), pp 531–554. New York: Plenum.

Hensler K (1992) Neuronal co-processing of course deviation and head movements in locusts. I. Descending deviation detectors. J Comp Physiol A Neuroethol Sens Neural Behav Physiol 171:257–271.

Hensler K, Rowell CHF (1990) Control of optomotor responses by descending deviation detector neurones in intact flying locusts. J Exp Biol 149:191–205.

Henze MJ, Labhart T (2007) Haze, clouds and limited sky visibility: polarotactic orientation of crickets under difficult stimulus conditions. J Exp Biol 210:3266–3276.

Homberg U (2004) In search of the sky compass in the insect brain. Naturwissenschaften 91:199–208.

Homberg U, Würden S, Dircksen H, Rao KR (1991) Comparative anatomy of pigment-dispersing hormone-immunoreactive neurons in the brain of orthopteroid insects. Cell Tissue Res 266:343–357.

Homberg U, Reischig T, Stengl M (2003) Neural organization of the circadian system of the cockroach *Leucophaea maderae.* Chronobiol Int 20:577–591.

Horváth G, Varjú D (2004) Polarized light in animal vision. Berlin: Springer.

Kien J (1976) Arousal changes in the locust optomotor system. J Insect Physiol 22:393–396.

Kien J, Fletcher WA, Altman JS, Ramirez J, Roth U (1990) Organization of intersegmental interneurons in the suboesophageal ganglion of *Schistocerca gregaria* (Forksal) and *Locusta migratoria migratorioides* (Reiche and Fairmaire) (Acrididae, Orthoptera). Int J Insect Morphol Embryol 19:35–60.

Labhart T (1996) How polarization-sensitive interneurones of crickets perform at low degrees of polarization. J Exp Biol 199:1467–1475.

Labhart T, Meyer EP (1999) Detectors for polarized skylight in insects: a survey of ommatidial specializations in the dorsal rim area of the compound eye. Microsc Res Tech 47:368–379.

Labhart T, Meyer EP (2002) Neural mechanisms in insect navigation: polarization compass and odometer. Curr Opin Neurobiol 12:707–714.

Lindauer M (1960) Time-compensated sun orientation in bees. Cold Spring Harbor Symp Quant Biol 25:371–377.

Longden KD, Krapp HG (2009) State-dependent performance of optic-flow processing interneurons. J Neurophysiol 102:3606–3618.

Mappes M, Homberg U (2004) Behavioral analysis of polarization vision in tethered flying locusts. J Comp Physiol A Neuroethol Sens Neural Behav Physiol 190:61–68.

Marder E, Calabrese RL, Nusbaum MP, Trimmer B (1987) Distribution and partial characterization of FMRFamide-like peptides in the stomatogastric nervous systems of the rock crab, *Cancer borealis*, and the spiny lobster, *Panulirus interruptus.* J Comp Neurol 259:150–163.

Mouritsen H, Frost BJ (2002) Virtual migration in tethered flying monarch butterflies reveals their orientation mechanisms. Proc Natl Acad Sci U S A 99:10162–10166.

Okada R, Sakura M, Mizunami M (2003) Distribution of dendrites of descending neurons and its implications for the basic organization of the cockroach brain. J Comp Neurol 458:158–174.

Olberg RM (1986) Identified target-selective visual interneurons descending from the dragonfly brain. J Comp Physiol A Neuroethol Sens Neural Behav Physiol 159:827–840.

Peters BH, Römer H, Marquart V (1986) Spatial segregation of synaptic inputs and outputs in a locust auditory interneurone. J Comp Neurol 254:34–50.

Pfeiffer K (2006) Coding of sky-compass information in neurons of the anterior optic tubercle of the desert locust *Schistocerca gregaria.* PhD thesis, Philipps University Marburg.

Pfeiffer K, Homberg U (2007) Coding of azimuthal directions via time-compensated combination of celestial compass cues. Curr Biol 17: 960–965.

Reppert SM, Zhu H, White RH (2004) Polarized light helps monarch butterflies navigate. Curr Biol 14:155–158.

Reppert SM, Gegear RJ, Merlin C (2010) Navigational mechanisms of migrating monarch butterflies. Trends Neurosci 33:399–406.

Rind FC (1990) A directionally selective motion-detecting neurone in the brain of the locust: physiological and morphological characterization. J Exp Biol 149:1–19.

Rind FC, Santer RD, Wright GA (2008) Arousal facilitates collision avoidance mediated by a looming sensitive visual neuron in a flying locust. J Neurophysiol 100:670–680.

Rowell CHF, Reichert H (1986) Three descending interneurons reporting deviation from course in the locust. II. Physiology. J Comp Physiol A Neuroethol Sens Neural Behav Physiol 158:775–794.

Sakura M, Lambrinos D, Labhart T (2008) Polarized skylight navigation in insects: model and electrophysiology of e-vector coding by neurons in the central complex. J Neurophysiol 99:667–682.

Schlurmann M, Hausen K (2007) Motoneurons of the flight power muscles of the blowfly *Calliphora erythrocephala*: structures and mutual dye coupling. J Comp Neurol 500:448–464.

Siegler MV, Phong MP, Pousman CA (1991) Motor neurons supplying hindwing muscles of a grasshopper: topography and distribution into anatomical groups. J Comp Neurol 311:342–355.

Sprayberry JD (2009) Responses of descending visually-sensitive neurons in the hawkmoth, *Manduca sexta*, to three dimensional flower-like stimuli. J Insect Sci 9:7.

Strausfeld NJ (1976) Atlas of an insect brain. Berlin: Springer.

Strausfeld NJ, Seyan HS (1985) Convergence of visual, haltere, and prosternal inputs at neck motor neurons of *Calliphora erythrocephala.* Cell Tissue Res 240:601–615.

Taube JS (2007) The head direction signal: origins and sensory motor integration. Annu Rev Neurosci 30:181–207.

Vitzthum H, Homberg U (1998) Immunocytochemical demonstration of locustatachykinin-related peptides in the central complex of the locust brain. J Comp Neurol 390:455–469.

Vitzthum H, Homberg U, Agricola H (1996) Distribution of Dip-allatostatin I-like immunoreactivity in the brain of the locust *Schistocerca gregaria* with detailed analysis of immunostaining in the central complex. J Comp Neurol 369:419–437.

Vitzthum H, Müller M, Homberg U (2002) Neurons of the central complex of the locust *Schistocerca gregaria* are sensitive to polarized light. J Neurosci 22:1114–1125.

von Philipsborn A, Labhart T (1990) A behavioural study of polarization vision in the fly, *Musca domestica.* J Comp Physiol A Neuroethol Sens Neural Behav Physiol 167:737–743.

Wehner R (1992) Arthropods. In: Animal homing (Papi F, ed), pp 45–144. London: Chapman and Hall.

Wehner R (2003) Desert ant navigation: how miniature brains solve complex tasks. J Comp Physiol A Neuroethol Sens Neural Behav Physiol 189:579–588.

Wehner R, Labhart T (2006) Polarisation vision. In: Invertebrate vision (Warrant E, Nilsson DE, eds), pp 291–348. Cambridge, UK: Cambridge UP.

Wehner R, Rossel S (1985) The bee's celestial compass: a case study in behavioural neurobiology. Fortschr Zool 31:11–53.

Wertz A, Borst A, Haag J (2008) Nonlinear integration of binocular optic flow by DNOVS2, a descending neuron of the fly. J Neurosci 28: 3131–3140.

Wertz A, Haag J, Borst A (2009a) Local and global motion preferences in descending neurons of the fly. J Comp Physiol A Neuroethol Sens Neural Behav Physiol 195:1107–1120.

Wertz A, Gaub B, Plett J, Haag J, Borst A (2009b) Robust coding of egomotion in descending neurons of the fly. J Neurosci 29:14993–15000.

Williams JLD (1975) Anatomical studies of the insect central nervous system: A ground-plan of the midbrain and an introduction to the central complex in the locust, *Schistocerca gregaria* (Orthoptera). J Zool 176:67–86.

Yamawaki Y, Toh Y (2009) Responses of descending neurons to looming stimuli in the praying mantis *Tenodera aridifolia.* J Comp Physiol A Neuroethol Sens Neural Behav Physiol 195:253–264.